This is the author's version of an article that has been published in this journal. Changes were made to this version by the publisher prior to publication.
The final version of record is available at http://dx.doi.org/10.1109/MCSE.2017.3421553

Wavelet-based Visual Analysis for Data Exploration

Alcebiades Dal Col, Paola Valdivia, Fabiano Petronetto, Fabio Dias,
Claudio T. Silva, *Senior Member, IEEE* and L. Gustavo Nonato, *Member, IEEE*

Abstract—
The conventional wavelet transform is widely used in image and signal processing, where a signal is decomposed into a combination of known signals. By analyzing the individual contributions, the behavior of the original signal can be inferred. In this article, the authors present an introductory overview of the extension of this theory into graph domains. They review the graph Fourier transform and graph wavelet transforms that are based on dictionaries of graph spectral filters, namely spectral graph wavelet transforms. Then, the main features of the graph wavelet transforms are presented using real and synthetic data.

Index Terms—Graph signal processing, spectral graph wavelet transforms, time-varying data.

1 Introduction

The theory of graph signal processing has emerged as a main alternative to analyze signals defined on the vertices of graphs [3]. It focuses on adapting tools and operators, such as Fourier and Wavelet transforms, to the context of graphs, opening a multitude of possibilities to the exploration and understanding of static and time-varying phenomena in irregular domains.

Similarly to the case of regular domains, most of the analysis derived from Graph Fourier (GFT) and Graph Wavelet Transforms (GWT) [2, 6, 5], relies on the processing of coefficients associated with certain basis functions defined on the vertices of a graph [1]. However, the irregular nature of graph domains makes the coefficients sensitive not only to the properties of the signal under analysis, but also to the topology of the graph. In fact, the topology of the graph directly impacts how the frequencies are spread in the graph Fourier domain, making the design of filters a more intricate task [4]. Filters designed without considering the distribution of frequencies may lead to wrong analysis and processing results. The issue of properly designing filters to operate with GFT and GWT becomes even more challenging for inexperienced users that are not usually aware of the nuances involved in the transforms. However, the sensitivity of the GFT and GWT to signal variation across irregular domains is an evident and noteworthy characteristic of these transforms, which can be used to understand phenomena related to daily life. For example, the street map of a city can be represented as a graph and the way the data under analysis varies across streets, from corner to corner, may reveal important aspects of city's dynamics.

In this paper we discuss some aspects of the GFT and GWT, providing examples of how the signal and the topology of the graph impact the computation of coefficients. Our goal is not to provide a rigorous treatment towards understanding the effect of the topology on GFT and GWT coefficients, but to shed some light on it to help inexperienced users in the use of these tools. In fact, the clear understanding of the synergy among GFT and GWT coefficients, graph topology, and the signal under analysis is still an open issue, which we consider out of the scope for this work.

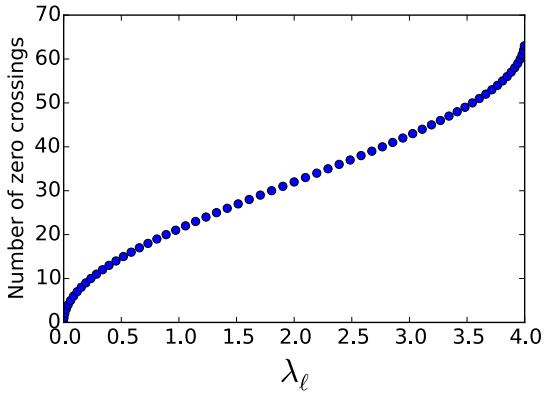

Fig. 1. Number of zero crossings, $|Z_G(u_\ell)|$, of the graph Laplacian eigenvectors u_ℓ, $\ell = 1,2,\ldots,64$ for a path graph with 64 nodes.

We present a set of controlled experiments, using real and synthetic data, to illustrate how the topology and signal can affect the result of GFT and GWT. We bring some intuition from the conventional Fourier and Wavelet theory to the more complex scenario of graph domains, relying on simple, but illustrative, examples showing the dissociation between spectral distribution and filter design in this context. We conclude this article with a real application that reveals the power of GFT and GWT in uncovering patterns and interesting phenomena hidden in the data.

2 Graph Wavelet Transforms

Let $G = (V, E, w)$ be a *graph* containing a node set $V = \{\tau_1, \tau_2, \ldots, \tau_n\}$, an edge set $E = \{(\tau_i, \tau_j) \,|\, \tau_i, \tau_j \in V, i \neq j\}$, and a weight function $w : E \to \mathbb{R}$ that associates a non-negative scalar to each edge of G. We assume that G is *connected*, for every pair of nodes, there is a path (sequence of edges such that any two sequential edges contain a node in common) connecting them.

The *weighted adjacency matrix* of G is the matrix $A = (a_{ij})$, where $a_{ij} = w(\tau_i, \tau_j)$ if $(\tau_i, \tau_j) \in E$ and $a_{ij} = 0$ otherwise. This matrix is used to define the (non-normalized) *graph Laplacian*, given by $L = D - A$, where $D = \mathrm{diag}(d_1, d_2, \ldots, d_n)$ is a diagonal matrix with entries $d_i = \sum_j a_{ij}$. The graph Laplacian is a real, symmetric, and semi-positive definite matrix, thus it has a complete set of orthonormal eigenvectors u_ℓ, with corresponding non-negative real eigenvalues λ_ℓ, $\ell = 1,2,\ldots,n$, which we consider ordered in non-decreasing order $0 = \lambda_1 < \lambda_2 \leq \cdots \leq \lambda_n$.

A signal defined on the nodes of G $f : V \to \mathbb{R}$ is a function that associates a real value $f(\tau_i)$ to each node $\tau_i \in V$. The graph Laplacian eigenvectors $u_\ell : V \to \mathbb{R}$ can be interpreted as signals on the graph G.

- *A. Dal Col is with ICMC - USP, Brazil. E-mail: alcebiades_dalcol@usp.br.*
- *P. Valdivia is with ICMC - USP, Brazil and INRIA, France. E-mail: paolalv@icmc.usp.br.*
- *F. Petronetto is with Federal University of Espirito Santo, Brazil. E-mail: fabiano.carmo@ufes.br*
- *F. Dias and C. Silva are with NYU, USA. E-mail: {fabio.dias,csilva}@nyu.edu.*
- *L. G. Nonato is with ICMC - USP, Brazil. E-mail: gnonato@icmc.usp.br.*

Manuscript received xx xxx. 201x; accepted xx xxx. 201x. Date of Publication xx xxx. 201x; date of current version xx xxx. 201x.
For information on obtaining reprints of this article, please send e-mail to: reprints@ieee.org.
Digital Object Identifier: xx.xxxx/TVCG.201x.xxxxxxx/

This is the author's version of an article that has been published in this journal. Changes were made to this version by the publisher prior to publication.
The final version of record is available at http://dx.doi.org/10.1109/MCSE.2017.3421553

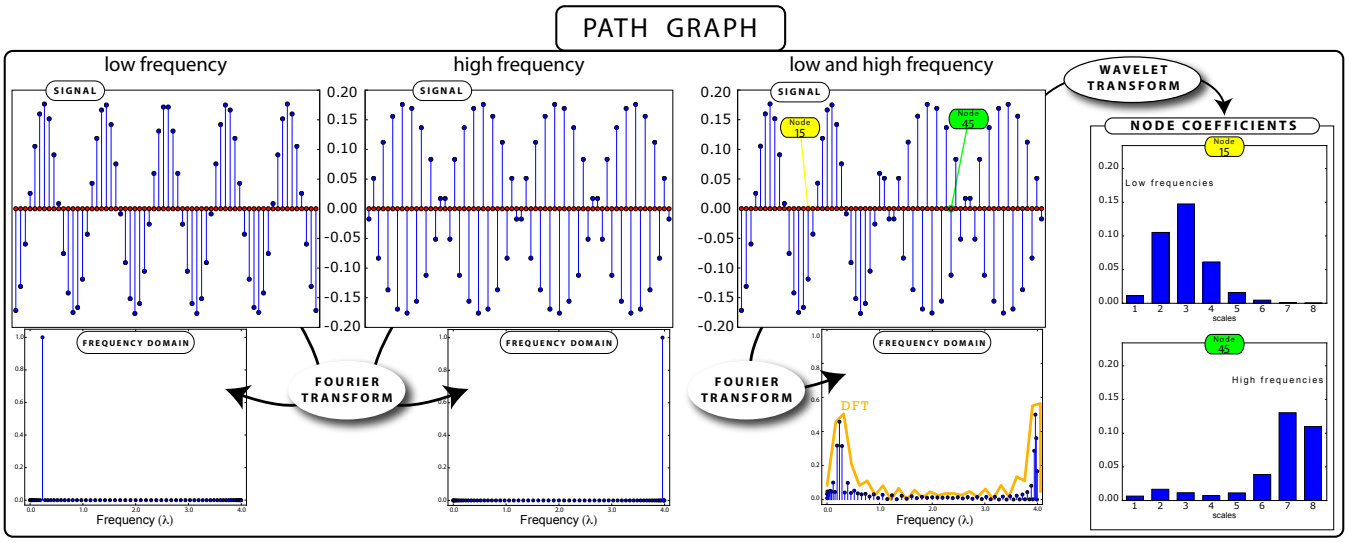

Fig. 2. **Signal:** Low frequency, high frequency, and f_0 signals defined on a path graph with 64 nodes. Signal f_0 is a combination of the low and high frequency signals. Red points represent the graph nodes and the height of the vertical blue lines correspond to the amplitude of the signal. **GFT:** The graph Fourier transforms are indicated by arrows. The graph Fourier transform corresponding to the signal f_0 indicates the presence of low and high frequencies. The yellow curve illustrates the discrete Fourier transform of f_0 when defined on the real line. **GWT:** The graph wavelet transform shows wavelet coefficients of nodes τ_{15} and τ_{45} for signal f_0.

Let $f : V \to \mathbb{R}$ be a signal defined on a graph G, the *zero crossings set* of f on G is given by:

$$Z_G(f) = \{(\tau_i, \tau_j) \in E \,|\, f(\tau_i) f(\tau_j) < 0\}. \tag{1}$$

$Z_G(f)$ is the set of edges connecting nodes where f has different signs (positive and negative). The larger the value $|Z_G(f)|$, the more f changes its sign across the graph. Figure 1 shows the number of zero crossings of the graph Laplacian eigenvectors u_ℓ as ℓ grows, assuming the eigenvectors are ordered in non-decreasing order of eigenvalues, for a path graph with 64 nodes. The eigenvectors associated with larger eigenvalues oscillate more throughout the graph. Therefore, the eigenvalues and eigenvectors of the graph Laplacian can be interpreted as frequencies and basis functions similarly to the Fourier theory, that is, the larger the frequency (eigenvalue) the more oscillatory the corresponding basis function (eigenvector).

Let $\Lambda = \{\lambda_1, \lambda_2, \ldots, \lambda_n\}$ be the set of eigenvalues, the *Graph Fourier Transform* (GFT) of a signal f, $\hat{f} : \Lambda \to \mathbb{R}$, is defined as:

$$\hat{f}(\lambda_\ell) = \langle u_\ell, f \rangle = \sum_{j=1}^{n} u_\ell(\tau_j) f(\tau_j). \tag{2}$$

Usually, the GFT is represented by a plot formed by the points $(\lambda_\ell, \hat{f}(\lambda_\ell))$, $\ell = 1, 2, \ldots, n$. Similarly to the conventional Fourier transform, the GFT reveals the frequencies present in a signal. High frequency coefficients $\hat{f}(\lambda_\ell)$ (when λ_ℓ is in the rightmost part of the spectrum) indicate that a signal varies abruptly in some regions of the graph, while low frequency coefficients suggest smooth signal variation. In order to illustrate this concept and show the relation with conventional Fourier transform, we consider a path graph (each node, except the two extreme ones, is adjacent to exactly two other nodes) with 64 nodes. We consider two eigenvectors as signals, one of low frequency and one of high frequency, as illustrated in Figure 2. The GFT of these signals is also depicted in Figure 2, corresponding to the spikes on the corresponding frequencies, the same behavior as in the conventional Fourier transform.

The GFT provides a global description of the signal behavior on the graph. For example, let f_0 be a signal defined as a combination of low and high frequency eigenvectors discussed above, as illustrated in Figure 2. The GFT of f_0, also shown in Figure 2, indicates the presence of low and high frequencies in the signal, suggesting that the signal has both smooth and abrupt variation. The yellow curve illustrates the magnitude of the conventional *Discrete Fourier Transform* (DFT) of f_0 when defined on the real line.

A graph spectral filter, or kernel, $\hat{g} : \Lambda \to \mathbb{R}$ is a function defined in the spectral domain that associates a scalar value $\hat{g}(\lambda_\ell)$ to each eigenvalue $\lambda_\ell \in \Lambda$. The GFT $\hat{f} : \Lambda \to \mathbb{R}$ can be seen as a particular instance of a graph spectral filter. A dictionary $\{\hat{g}_m\}_{m=1,2,\ldots,M}$ is a set of graph spectral filters $\hat{g}_m : \Lambda \to \mathbb{R}$, $m = 1, 2, \ldots, M$, where M is the number of kernels in the dictionary. Given a signal f and a dictionary $\{\hat{g}_m\}_{m=1,2,\ldots,M}$, the *Graph Wavelet Transform* (GWT) $W_f : \{1, 2, \ldots, M\} \times V \to \mathbb{R}$ is defined as:

$$W_f(m, \tau_j) = \sum_{\ell=1}^{n} \hat{g}_m(\lambda_\ell) \widehat{f}(\lambda_\ell) u_\ell(\tau_j). \tag{3}$$

By varying m while keeping τ_j fixed, we obtain M wavelet coefficients associated to τ_j. Moreover, the product $\hat{g}_m(\lambda_\ell)\widehat{f}(\lambda_\ell)$, on the right of Equation 3, shows that each coefficient $W_f(m, \tau_j)$ is obtained by modulating $\widehat{f}(\lambda_\ell)$ by the kernel $\hat{g}_m(\lambda_\ell)$. Interpreting $\hat{g}_m$ as a band-pass filter, where small values of m correspond to low-pass and larger values to high-pass filters, the coefficients encode the behavior of the signal in each node. To illustrate this fact, consider the signal f_0 as defined above (Figure 2). Figure 2 depicts the wavelets coefficients associated to nodes τ_{15} and τ_{45}, where the taller the bar plot, larger the coefficient. The coefficients corresponding to low frequencies ($m \leq 4$) in node τ_{15} are larger than high frequency coefficients, reflecting the fact that the signal in node τ_{15} is smoother. In contrast, larger coefficients appear in high frequencies, indicating that the signal oscillates more abruptly around in node τ_{45}.

3 Understanding the Interplay among Spectrum, Topology, and Coefficients

In the previous section we showed how the behavior of a signal affects the graph Fourier and graph wavelet coefficients. However, in the examples in Figure 2 the graph defining the signal domains is essentially the same as a discretization of the real line, that is, the graph topology is fairly regular. In scenarios where the graph is irregular, not only the signal but also the graph topology plays a role in the computation of the coefficients, as we discuss in the following.

Comet experiment. A *comet graph* is formed by combining a path graph and a star graph, the latter centered in one of the extremities of the path graph, as illustrated at the top left of Figure 3. The

This is the author's version of an article that has been published in this journal. Changes were made to this version by the publisher prior to publication.
The final version of record is available at http://dx.doi.org/10.1109/MCSE.2017.3421553

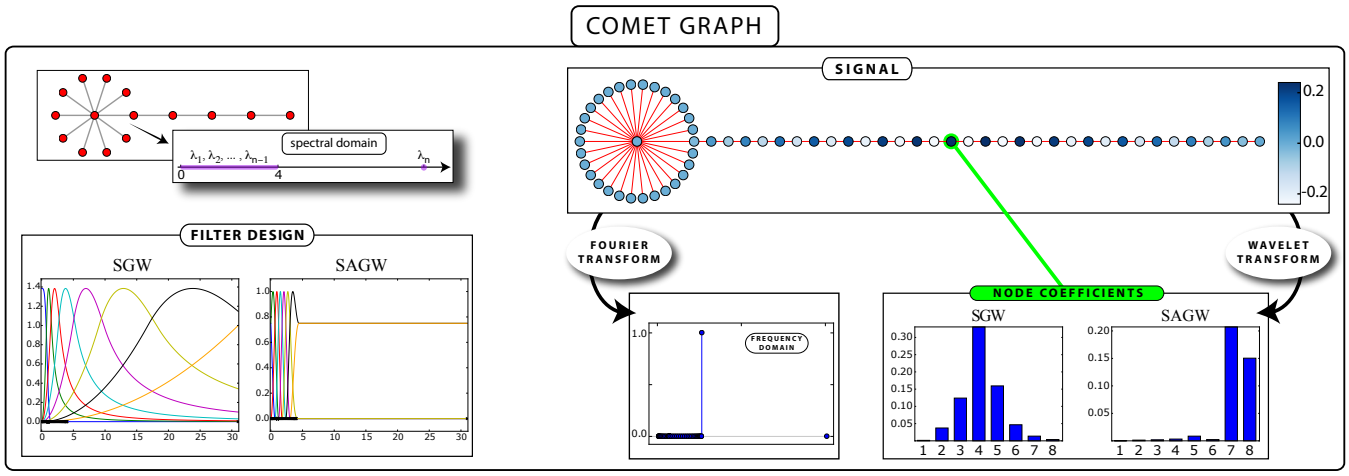

Fig. 3. **Top left:** Comet graph and corresponding spectral distribution. The purple interval concentrate $n-1$ eigenvalues. The highest eigenvalue is isolate; the greater the degree of star graph, the greater the distance. **Bottom left:** Graph spectral filters for the SGW and SAGW dictionaries. The SAGW filters adapt to regions with larger spectral density. The x marks on the horizontal axis represent the graph Laplacian spectrum of a comet graph. **Top right:** Second largest graph Laplacian eigenvector defined on a comet graph with 64 nodes. The color associated to the graph nodes encodes the signal. **Bottom right:** Corresponding GFT and GWT coefficients of the specified node. The GFT reveals the presence of high global frequency. The GWT was produced using the SGW and SAGW dictionaries.

eigenvalues of the graph Laplacian of a comet graph present a peculiar distribution, as the difference between the two largest eigenvalues is much larger than the difference between the other eigenvalues (Figure 3 top left). Although the second largest eigenvalue is distant from the largest eigenvalue, it corresponds to the second highest frequency in the spectrum of the comet graph.

As discussed in the previous section, the GWT (Equation (3)) relies on a dictionary of kernel functions $\{\hat{g}_m\}_{m=1,2,\ldots,M}$ defined in the spectral domain. Each kernel $\hat{g}_m$ operates as a filter in the spectral domain, thus the distribution of the eigenvalues impacts in which frequencies are filtered. For instance, the bottom left of Figure 3 shows two dictionaries employed in the definition of the Spectral Graph Wavelet (SGW) [1] and Spectrum-Adapted Graph Wavelet (SAGW) [4], both defined in the same spectral domain. The filtering result and the wavelet coefficients derived from each dictionary are very different, since SGW kernels are designed to evenly cover the spectral domain, while the kernels used by SAGW adapt to the spectral distribution. As one can clearly see at the bottom left of Figure 3, when eigenvalues are not evenly distributed in the spectral domain, as is the case of the comet graph, the SAGW dictionary better fits the frequency bands. In fact, the SAGW dictionary forms a tight frame that allows interpreting the squared magnitudes of the coefficients as an energy density function [4], making the understanding of wavelets coefficients an easier task.

In order to further illustrate this point, we created a comet graph with 64 nodes with the star extremity containing 30 nodes. The signal is defined as the second largest graph Laplacian eigenvector (Figure 3 top right). The GFT of this signal is illustrated at the bottom right of Figure 3. As expected, the GFT presents a spike in the second to last eigenvalue. The wavelet coefficients of the highlighted node, computed via SGW and SAGW, are also illustrated at the bottom right of Figure 3. The SGW dictionary led to wavelet coefficients with dominant frequencies in the central scales, not properly characterizing the high frequency nature of the signal under analysis. In contrast, SAGW dictionary generated wavelet coefficients with larger intensity in the scales related to high frequencies, better capturing the pattern of variation of the signal.

Minnesota experiment. The synthetic examples above showed how the topology of a graph can affect the wavelet coefficients. Lets analyze now how patterns in the signal are captured by wavelet coefficients. Consider the Minnesota road graph depicted in Figure 4. We divide the graph into three different regions R_1, R_2, and R_3, colored as blue, green, and red in the cluster panel of Figure 4. A signal with a different dominant frequency band is assigned to each region, resulting in a global signal defined as:

$$f := \sum_{j=1}^{3} f_j/||f_j||_\infty \quad \text{where} \tag{4}$$

$$f_j(\tau_i) = \begin{cases} \sum_{\ell \in I_j} u_\ell(\tau_i) & \text{if } \tau_i \in R_j \\ 0 & \text{otherwise} \end{cases} \tag{5}$$

where I_j are the indices of the eigenvalues lying in the intervals $[a_j, b_j]$ given by $[0.0, 0.08]$, $[2.0, 2.5]$, and $[5.0, 7.0]$. The ranges of the intervals were chosen according to the distribution of the eigenvalues as illustrated in the eigenvalues panel of Figure 4. Therefore, region R_1 (blue) has a low frequency signal, since it is the summation of eigenvectors corresponding to eigenvalues in the low frequency region of the spectrum. Similarly, the signal in R_2 (green) and R_3 (red) correspond to the summation of eigenvectors associated with high and median frequency eigenvalues, respectively. The signal panel of Figure 4 shows the signal f as defined above. The node coefficients panel of Figure 4 illustrates representative wavelet coefficients for each region computed using the SAGW dictionary. Notice that the behavior of the coefficients corresponds to exactly what we expect. However, the coefficients corresponding to representative nodes are observed mainly in the middle of each region. Nodes close to the boundary between regions tend to have a more mixed behavior, as illustrated in the node coefficients panel of Figure 4.

4 Time-Varying Data

The discussion above assumes a static signal defined on the nodes of the graph. However, in many applications data varies with time, resulting in a time series associated to each node [6]. One of the possible options to create a graph representing time-varying data is using the Cartesian product of graphs.

Given two graphs $G = (V_G, E_G)$ and $H = (V_H, E_H)$, the Cartesian product between them is a graph $G \times H$ with node set $V_G \times V_H = \{\tau_i \iota_j \,|\, \tau_i \in V_G, \iota_j \in V_H\}$ and edges connecting nodes $\tau_i \iota_j$ and $\tau_k \iota_l$ if only if $\tau_i = \tau_k$ and ι_j is adjacent to ι_l in H, or $\iota_j = \iota_l$ and τ_i is adjacent to τ_k in G. If H is a path graph, the Cartesian product graph $G \times H$, as illustrated in Figure 5, corresponds to "stacked" copies of G with edges connecting corresponding nodes in adjacent copies of G. Each

This is the author's version of an article that has been published in this journal. Changes were made to this version by the publisher prior to publication.
The final version of record is available at http://dx.doi.org/10.1109/MCSE.2017.3421553

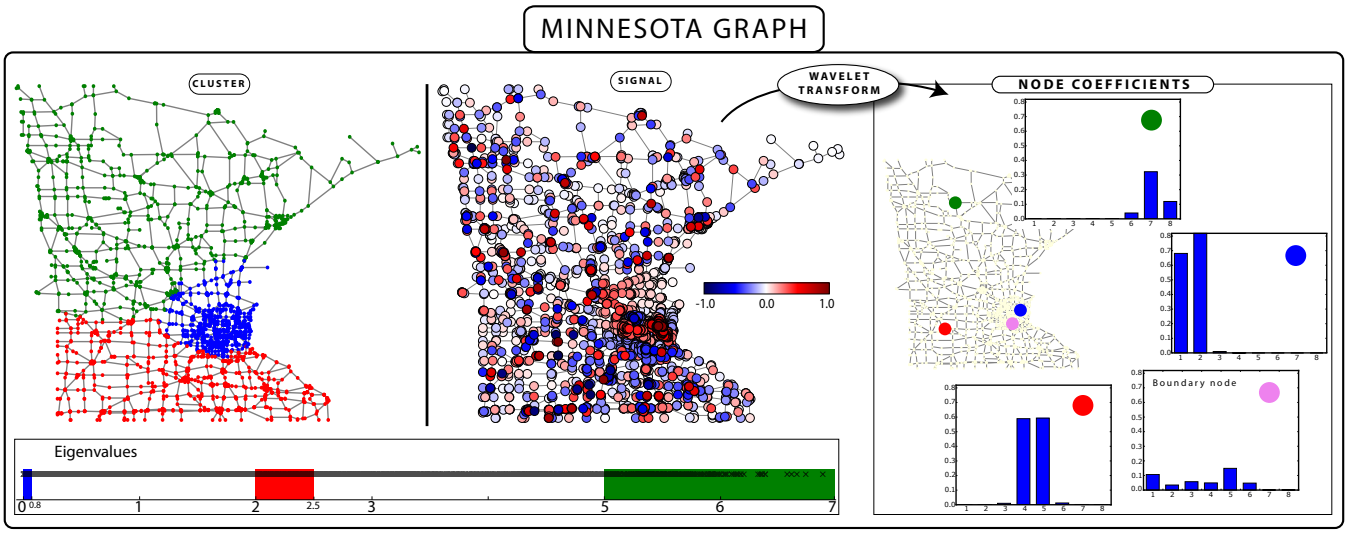

Fig. 4. **Left:** The Minnesota road graph divided into three different regions (cluster) and the signal defined on the Minnesota road graph. The signal is formed so each region has a dominant frequency interval, which are highlighted on eigenvalues panel. **Right:** Wavelet coefficients of representative nodes in the regions on the left (dot colors) and one node close to the boundary between regions (pink). The bar plots represent wavelet coefficients, where the coefficients are ordered from smaller to higher frequencies. The GWT was produced using the SAGW dictionary.

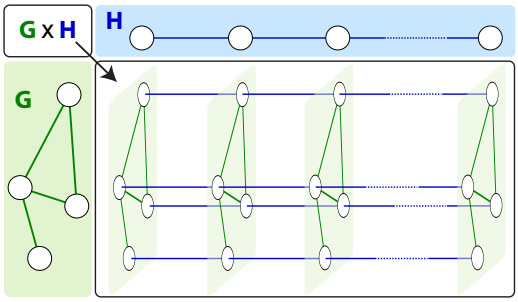

Fig. 5. Spatio-temporal data modeled by the Cartesian product between two graphs spatial G and temporal H.

copy of G is interpreted as a time slice of the temporal data, enabling the use of GFT and GWT on $G \times H$ to analyze time varying data.

In the Cartesian graph, the coefficients derived from GFT and GWT capture spatial and temporal behavior of the signal, making their interpretation more intricate than in the static case. In order to gain intuition, we design a Cartesian graph $G \times H$ where G is as depicted in the leftmost panel in Figure 6 and H is a path graph with twenty nodes; $G \times H$ comprises twenty time slices of a time-varying signal defined on its nodes. We also craft four different time-varying signals on $G \times H$ denoted as $f_i, i = 1,2,3,4$. The signal f_1 is defined with a spike (value equal 1) in the node $\tau_a \iota_{10}$ of $G \times H$, vanishing in the remaining nodes. The nodes τ_a and ι_{10} are enhanced in the leftmost panel in Figure 6. In other words, f_1 has a spike in the node τ_a in time slice ι_{10}. The signal f_2 is defined as a "spatial" Gaussian centered in $\tau_a \iota_{10}$, assigning values for nodes in the neighborhood of τ_a in time slice 10 and zero in other time slices. The signal f_3 is defined as a "temporal" Gaussian centered in $\tau_a \iota_{10}$, assigning values for nodes $\tau_a \iota_j$, $j = 1,\ldots,20$ and zero elsewhere. Finally, f_4 is the combination of a Gaussian over time centered at $\tau_a \iota_{10}$ and Gaussians in all time slices with spikes in $\tau_a \iota_j$, $j = 1,\ldots,20$.

The bar plots in the center panel of Figure 6 show the wavelet coefficients associated to the node $\tau_a \iota_{10}$. The coefficients correctly reflect the behavior of the functions in the selected node. In the top left bar plot, corresponding to f_1, there is a concentration of larger coefficients in high scales, indicating that f_1 has a high frequency in $\tau_a \iota_{10}$. The smoothness of f_2 and f_4 in $\tau_a \iota_{10}$ are also evident in the bar plots on the bottom row. The bar plot on the top right, which reflects the behavior of f_3 around $\tau_a \iota_{10}$, does not clearly depict the temporal smoothness of f_3, as the amplitude of the coefficients of f_3 in $\tau_a \iota_{10}$ are similar to those of f_1. The reason for GWT not properly capturing the temporal smoothness of f_3 in $\tau_a \iota_{10}$ is the topology of $G \times H$, which contains many more spatial than temporal edges around $\tau_a \iota_{10}$. In fact, there are only two temporal edges with ends in $\tau_a \iota_{10}$. Therefore, the spatial distribution of f_3 around $\tau_a \iota_{10}$ impacts more the wavelet coefficients than its temporal distribution. This fact becomes obvious when we remove some spatial edges from the neighborhood of $\tau_a \iota_{10}$, triggering a shift of the coefficients to low frequency scales, as illustrated in the rightmost panel of Figure 6.

Manhattan taxi pick-ups. Discussion above raises the question whether it is worth using the Cartesian product graph. Would results be similar if GWT analysis were applied in each time slice independently? We answer these questions through a real application scenario involving taxi pick-ups in downtown Manhattan.

The left panel of Figure 7 depicts the street map of downtown Manhattan with corners colored by the number of taxi pick-ups in August 12, 2013, 07:30 to 08:00. The left panel of Figure 7 also shows the number of the taxi pick-ups at the corner of 8th Avenue with 41st Street at 07:00-07:30, 07:30-08:00, and 08:00-08:30 consecutive time slices (t_{i-1}, t_i, t_{i+1}). There are large spatial variations in the number of pick-ups on the corners of 41st Street near 8th Avenue in all time slices. By analyzing the (spatial) wavelet coefficients at the node 8th-41st at 07:30 to 08:00 time slice (leftmost column in the right panel of Figure 7) there is a predominance of mid and high frequency. However, the number of taxi pick-ups does not vary drastically among the adjacent time slices. Therefore, considering the temporal variation, the signal is smooth. Computing the (spatio-temporal) wavelet coefficients at the node 8th-41st at 07:30 to 08:00 time slice, but considering now the Cartesian product graph, that is, the three time slices are connected by temporal edges, we obtain the distribution of coefficients shown on the leftmost column in the right panel of Figure 7. The coefficients tend to concentrate in the low frequency scales, showing that when the spatial and temporal information are considered simultaneously, the signal tends to be of low frequency. Center and rightmost columns of Figure 7 correspond to the same analysis but considering two other corners, where a shift of the coefficients to low frequency also take place when temporal edges are considered.

From the provided experiments, the Cartesian product graph is more suitable to handle spatio-temporal data via GFT and GWT, better

This is the author's version of an article that has been published in this journal. Changes were made to this version by the publisher prior to publication.
The final version of record is available at http://dx.doi.org/10.1109/MCSE.2017.3421553

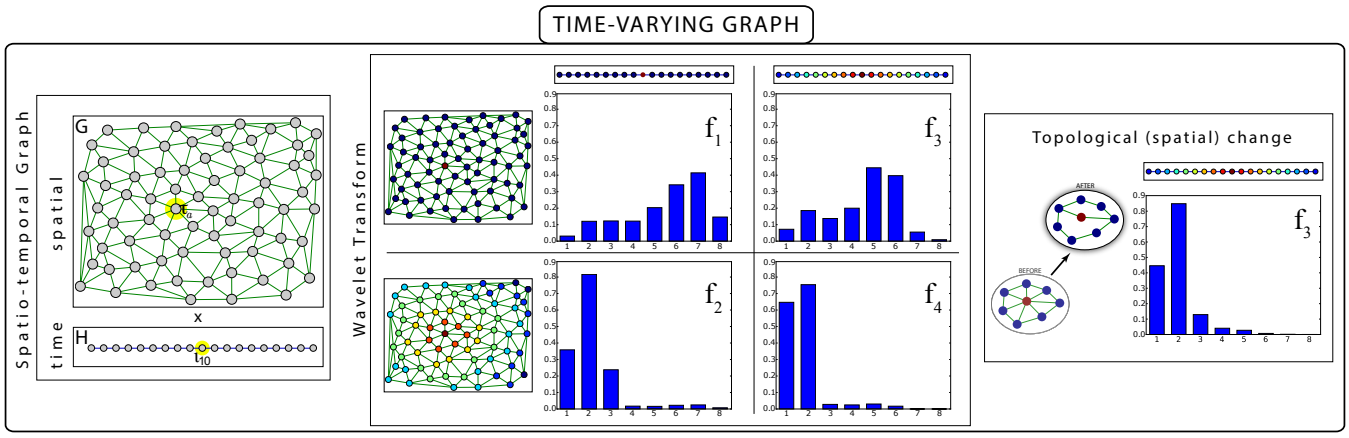

Fig. 6. **Left:** Graphs spatial G and temporal H. **Center:** Wavelet coefficients of the node $\tau_a \iota_{10}$ for the functions f_i, $i = 1,2,3,4$. **Right:** Wavelet coefficients of the node $\tau_a \iota_{10}$ for the functions f_3 after edges removal. The GWT was produced using the SAGW dictionary.

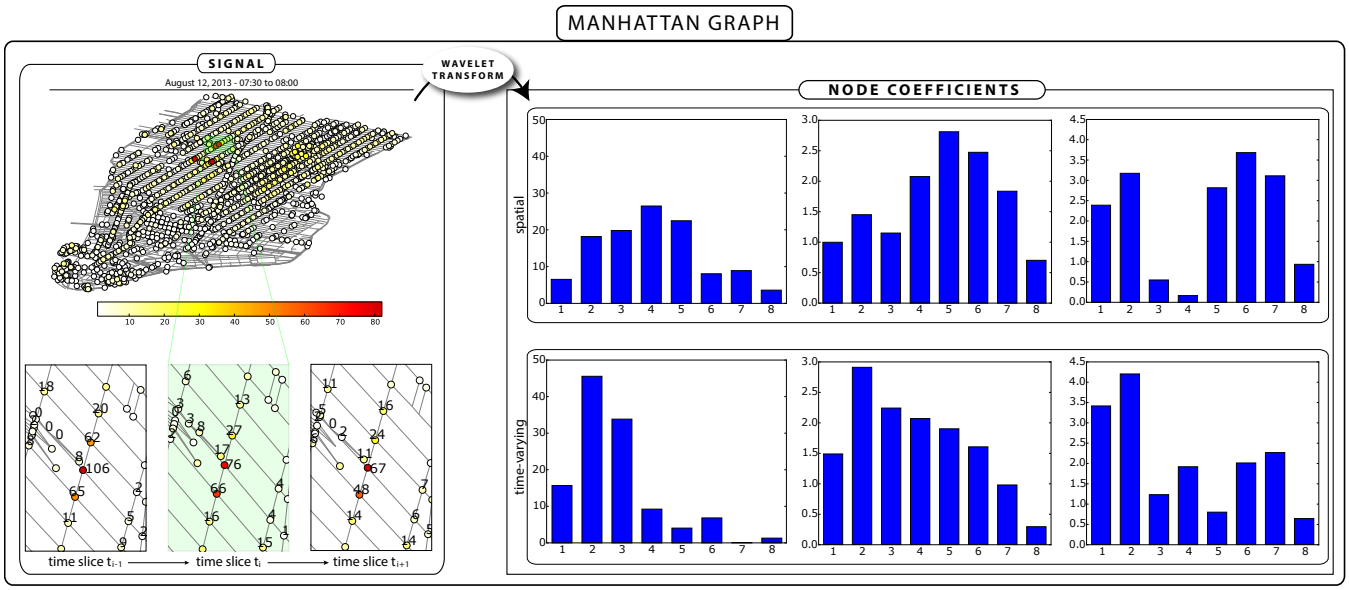

Fig. 7. **Left:** Taxi pick-ups in downtown Manhattan on August 12, 2013, 07:30 to 08:00 (top) and at the corner of 8th Avenue with 41st Street at 07:00-07:30, 07:30-08:00, and 08:00-08:30 consecutive time slices (t_{i-1}, t_i, t_{i+1})(bottom). **Right:** Spatial (top) and spatio-temporal (bottom) wavelet coefficients of the nodes on the corner of 8th Avenue with 41st Street (left), Church Street with Duane Street (center), and 6th Avenue with 53rd Street (right) corresponding to August 12, 2013, 07:30 to 08:00. The GWT was produced using the SAGW dictionary.

capturing properties of the signal, whether they are spatial or temporal.

5 Conclusion

We have shown the sensitivity of the GFT and GWT to signal variation across irregular domains. These transforms gracefully combine topology with the data under analysis, such that they can be used to understand phenomena related to daily life. For instance, a homogeneous number of taxi pick-ups across the street map of a city suggests a large event happening in the city, while a more heterogeneous pattern can lead us to influential localities. Further, the temporal evolution of data can be incorporated in the process in order to use GWT properties in spatio-temporal analyses.

Graph signal processing is still in its earlier days and much has to be done in order to make it accessible to inexperienced users from different fields. As we have shown in this article, many issues are still open, including how to change the edge weights to mitigate the impact of the topology in the graph Fourier coefficients and graph wavelet coefficients. Other interesting problem is how to design filters with particular properties such as boundary detection filters, which could be useful to perform unconventional clustering in spatio-temporal data.

Acknowledgments

Grants 2011/22749-8, 2013/14089-3, 2014/12815-1, 2015/03330-7, 2016/04391-2, and 2016/04190-7 from São Paulo Research Foundation (FAPESP). The views expressed are those of the authors and do not reflect the official policy or position of the São Paulo Research Foundation.

References

[1] D. K. Hammond, P. Vandergheynst, and R. Gribonval. Wavelets on graphs via spectral graph theory. *Applied and Computational Harmonic Analysis*, 30(2):129–150, 2011.

[2] D. M. Mohan, M. T. Asif, N. Mitrovic, J. Dauwels, and P. Jaillet. Wavelets on graphs with application to transportation networks. In *IEEE International Conference on Intelligent Transportation Systems*, pages 1707–1712. IEEE, 2014.

[3] D. I. Shuman, S. K. Narang, P. Frossard, A. Ortega, and P. Vandergheynst. The emerging field of signal processing on graphs: Extending high-

dimensional data analysis to networks and other irregular domains. *IEEE Signal Processing Magazine*, 30(3):83–98, 2013.

[4] D. I. Shuman, C. Wiesmeyr, N. Holighaus, and P. Vandergheynst. Spectrum-adapted tight graph wavelet and vertex-frequency frames. *IEEE Transactions on Signal Processing*, 63(16):4223–4235, 2015.

[5] N. Tremblay and P. Borgnat. Graph wavelets for multiscale community mining. *IEEE Transactions on Signal Processing*, 62(20):5227–5239, 2014.

[6] P. Valdivia, F. Dias, F. Petronetto, C. T. Silva, and L. Nonato. Wavelet-based visualization of time-varying data on graphs. In *IEEE Conference on Visual Analytics Science and Technology*. IEEE, 2015.